

This manuscript has been submitted for publication in the journal CHEMICAL GEOLOGY. Please note that, despite having undergone two rounds of peer-review at the journal EARTH AND PLANETARY SCIENCE LETTERS, the manuscript has yet to be formally accepted for publication. Subsequent versions of this manuscript may have slightly different content. Please feel free to contact any of the authors; we welcome feedback

## Oxidized Mantle Sources of HIMU and EM-type Ocean Island Basalts

Robert W. Nicklas<sup>1\*</sup>, Rachel K. M. Hahn<sup>1</sup>, Lori N. Willhite<sup>2</sup>, Matthew G. Jackson<sup>3</sup>,  
Vittorio Zanon<sup>4</sup>, Ricardo Arevalo Jr.<sup>2</sup> and James M.D. Day<sup>1</sup>

<sup>1</sup>Scripps Institution of Oceanography, University of California San Diego, La Jolla, CA, 92093,  
USA

<sup>2</sup>Department of Geology, University of Maryland College Park, College Park, MD, 20742, USA

<sup>3</sup>Department of Earth Science, University of California Santa Barbara, Santa Barbara, CA,  
93106, USA

<sup>4</sup>Instituto de Investigação em Vulcanologia e Avaliação de Riscos, Universidade dos Açores,  
Rua Mãe de Deus, 9500-321 Ponta Delgada, Portugal

\*Corresponding author: R. Willie Nicklas: [rnicklas@ucsd.edu](mailto:rnicklas@ucsd.edu)

5653 Words (Abstract 231, Supplement 2189), 82 References, 3 Figures, 4 Tables

For submission to *Chemical Geology*

8/31/2021

**1 Abstract:**

2           Oxygen fugacity ( $fO_2$ ) is a fundamental variable in igneous petrology with utility as a  
3 potential tracer of recycled surficial materials in the sources of mantle-derived lavas. It has been  
4 postulated that ocean island basalts (OIB) have elevated  $fO_2$  relative to mid-ocean ridge basalts  
5 (MORB) owing to more oxidized source regions. To clarify this issue, trace-element systematics  
6 of olivine grains are reported from OIB lavas with HIMU (high- $\mu$ ; Mangaia, Canary Islands),  
7 enriched mantle (EM; Samoa; São Miguel, Azores Islands) and depleted MORB mantle (DMM;  
8 Pico, Azores) Sr-Nd-Pb-Os isotopic signatures, to constrain the  $fO_2$  of each magmatic system.  
9 Despite sampling distinct mantle reservoirs based on radiogenic isotope systematics, these OIB  
10 suites show similar  $fO_2$ , ranging from +1.5 to +2.9  $\Delta FMQ$ , with an average of  $2.0 \pm 0.7 \Delta FMQ$ ,  
11 significantly higher than MORB at  $+0.6 \pm 0.2 \Delta FMQ$  using the same oxybarometer. OIBs show no  
12 correlation between  $fO_2$  and bulk rock isotopic ratios or parental magma compositions. The lack  
13 of correlations with isotopic signatures likely results from radiogenic isotope signatures being  
14 hosted in volumetrically minor trace element enriched mantle lithologies, while  $fO_2$  reflects the  
15 volumetrically dominant mantle component. Higher  $fO_2$  in OIB relative to MORB implies a  
16 uniformly oxidizing plume source mantle that may be the result of either a common oxidized  
17 oceanic crust-rich reservoir parental to all modern plume lavas, or preservation of un-degassed  
18 and oxidized mantle domains formed early in Earth history.

19

**20 Introduction**

21           Oxygen fugacity ( $fO_2$ ) is an intensive variable in igneous petrology that controls the  
22 geochemical behavior of redox-sensitive elements such as Fe, V, Cr, S, C and H. It is defined as

23 the chemical potential of molecular oxygen ( $O_2$ ) in equilibrium with an igneous system and, like  
24 all equilibria, oxygen fugacity depends on temperature and pressure. It is therefore normally  
25 discussed in igneous petrology relative to mineral redox buffers, with the most common being  
26 the fayalite-magnetite-quartz, or FMQ buffer (Lindsley, 1991). Oxygen fugacity varies significantly  
27 in natural Earth systems by ~nine orders of magnitude, from the reduced metallic core to an  
28 atmosphere that contains ~20% molecular  $O_2$ . Igneous systems also show large variations in  $fO_2$ ,  
29 with arc basalts and alkaline continental basalts showing systematically higher  $fO_2$  relative to  
30 plume and ridge basalts (Carmichael, 1991; Brounce et al. 2014). Oxygen fugacity in arc basalts is  
31 elevated by ~+1 to +5 log units  $\Delta FMQ$  above ambient mantle, although it is currently debated  
32 whether the high value of arc basalts results from subduction-related metasomatism of their  
33 mantle source, or from differentiation and degassing processes (Lee et al. 2005; Kelley and  
34 Cottrell, 2009; Brounce et al. 2014; Tang et al. 2018).

35 Oxygen fugacity is traditionally constrained in volcanic rocks using the  $Fe^{+3}/\Sigma Fe$  ratio of  
36 volcanic glasses coupled with the experimental formulation of Kress and Carmichael (1991). The  
37  $Fe^{+3}/\Sigma Fe$  ratio of volcanic glasses is determined in several ways, including wet chemistry and  
38 Mössbauer spectroscopy. X-ray Absorbance Near-Edge Spectroscopy (XANES) has recently  
39 allowed for high spatial resolution coupled with relatively fast sample throughput (Cottrell et al.  
40 2011; 2013; Moussallam et al. 2014; 2016; 2019; Brounce et al. 2014). However, XANES  
41 qualitative analyses of hydrous glasses and melt inclusions can be compromised by beam damage  
42 (Cottrell et al. 2018). Additionally, it has been shown that  $Fe^{+3}/\Sigma Fe$  ratio of melts can change on  
43 the order of minutes by interaction with atmospheric oxygen (Helz et al. 2017). Due to these  
44 challenges and issues, as well as the low preservation potential of pristine volcanic glasses,

45 alternative methods of determining magmatic  $fO_2$ , such as V/Sc and Zn/Fe ratios in bulk rocks  
46 (Lee et al. 2005; 2010), as well as the partitioning of V into olivine (Canil, 1997; Mallmann and  
47 O'Neill, 2009; 2013; Nicklas et al. 2018; 2019; 2021), have been developed. The oxidation state  
48 of vanadium in magmas varies from  $V^{+3}$  to  $V^{+5}$ ; the former being much more compatible in olivine,  
49 regardless of temperature, pressure and melt composition (Canil, 1997; Wang et al. 2019). The  
50 most important advantage of Vanadium-in-olivine oxybarometry over XANES Fe oxybarometry,  
51 is the possibility to obtain  $fO_2$  values of the melt at the first crystallization of primitive olivine, in  
52 many cases prior to any magmatic degassing. In contrast, XANES measures the  $fO_2$  as glass  
53 quenches, after the melt might have been modified by degassing and or assimilation processes.  
54 Additionally, V-in-olivine oxybarometry values are relatively hard to reset, as V diffusion in olivine  
55 is fairly slow with a diffusion coefficient on the order of  $10^{-14}$  m<sup>2</sup>/s (Chakraborty, 2010). This  
56 method can give erroneous results however, if the measured olivines are xenocrysts and did not  
57 crystallize from the rock in which they are found. Vanadium-in-olivine oxybarometry can be  
58 readily applied to primitive olivine-phyric lavas from a variety of settings.

59 In contrast to arc basalts, the  $fO_2$  of ocean island basalts (OIB) has only recently received  
60 significant attention. It has been postulated, based on XANES measurements in glassy melt  
61 inclusions, that Hawaiian basalts are oxidized relative to mid-ocean ridge basalts (MORB),  
62 although degassing of sulfur has led to substantial modification of their observed  $fO_2$   
63 (Moussallam et al. 2016; Brounce et al. 2017). A similar argument for degassing of sulfide and  
64 oxidation has also been demonstrated for intraplate alkaline lavas from Mt Erebus in Antarctica  
65 (Moussallam et al. 2014). The high values of  $fO_2$  (relative to MORB) measured in spinel grains  
66 hosted in residual mantle xenoliths from Cape Verde also suggest an oxidized mantle source for

67 Cape Verde magmas (Ryabchikov et al. 1995). Basaltic glasses from the Reykjanes Ridge adjacent  
68 to Iceland show a positive correlation between oxygen fugacity and proxies for geochemical  
69 enrichment, suggesting that significant amounts of oxidized surficial material are present within  
70 the Iceland plume (Shorttle et al. 2015; Novella et al. 2020). The idea that OIB source mantle is  
71 uniformly oxidized was extended by Moussallam et al. (2019) using new XANES measurements  
72 of melt inclusions of Cape Verde and the Canary Islands, along with a compilation of existing data  
73 from Mt. Erebus, Hawaii and Iceland. They showed a strong correlation of  $\text{Fe}^{+3}/\Sigma\text{Fe}$  ratio with  
74 volatile concentrations, especially S, suggesting that undegassed OIB lavas have  $f\text{O}_2$  of  $\sim+2$  log  
75 units from the FMQ buffer, substantially higher than MORB, which are close to FMQ (Berry et al.  
76 2018). However, this XANES method only gives a minimum  $f\text{O}_2$ , as even the most oxidized glasses  
77 may have experienced some sulfur degassing. Vanadium-in-olivine oxybarometry offers an  
78 earlier ‘snapshot’ of the  $f\text{O}_2$  of such lavas, potentially enabling a better approximation of the  
79 oxygen fugacity of OIB mantle. In order to examine the  $f\text{O}_2$  of OIB, and to determine whether  
80 their source is oxidized relative to the MORB source we applied V-in-olivine oxybarometry to a  
81 diverse set of OIB lavas from several different hotspots that are considered to contain recycled  
82 crustal components.

83

## 84 **Samples and Methods**

85 Olivines from twenty OIB lava samples were selected for trace element analysis. The lavas  
86 sample OIB localities with Sr-Nd-Pb-Os isotope signatures attributed to the recycling of oceanic  
87 or continental crustal sources and come from the Canary Islands, the Azores, Samoa, and  
88 Mangaia in the Cook Islands. Critically, Mangaia lavas show the highest  $^{206}\text{Pb}/^{204}\text{Pb}$  of any OIB

89 and thus represent the HIMU endmember (high- $\mu$ : high long-term  $^{238}\text{U}/^{204}\text{Pb}$ ) (Woodhead, 1996),  
90 while Samoan lavas represent the EM2 (Enriched Mantle) isotopic endmember (Jackson et al.  
91 2007a). The Canary Island lavas are 'HIMU-type' (Day et al., 2010), and samples from the same  
92 Canary Island volcanos have also been measured by Moussallam et al. (2019) by XANES. The  
93 Azores samples span a range of compositions from enriched mantle (EM)-like (eastern São  
94 Miguel; Elliot et al. 2007), to akin to MORB-like lavas (Pico; Waters et al., 2020). Background  
95 details about the samples are given in the *Supplementary Information*.

96 Vanadium-in-olivine oxybarometry relies upon the experimentally constrained  
97 relationship between  $D_{\text{V}}^{\text{olivine/melt}}$  and  $f\text{O}_2$ . If the concentration of V in olivine can be measured,  
98 and the V concentration of the parental melt of the olivine can be constrained,  $f\text{O}_2$  can be  
99 calculated. Concentrations of trace elements, including V, in the cores of primitive olivine crystals  
100 were measured using laser ablation inductively coupled plasma mass spectrometry (LA-ICP-MS).  
101 The analytical details can be found in the *Supplementary Information*. Calculation of parental  
102 magma compositions used previously published bulk rock data and the method of (Nicklas et al.  
103 2021) and are detailed in the *Supplementary Information*. In short, literature bulk rock data were  
104 used with the major element composition of the analyzed olivine to calculate the MgO content  
105 of the parental magma to the olivine. The method assumes FeO in the bulk rock samples are  
106 equal to that in the parental magmas, and this assumption has at most a secondary effect on the  
107 resulting  $f\text{O}_2$  values. The measured composition of the olivine was then subtracted from the bulk  
108 rock concentrations until it was in equilibrium with the olivine. This calculation was done for all  
109 major elements and for V, to establish the parental magma composition. The partition coefficient  
110 was then calculated using the average olivine V concentration and the modeled parental magma

111 V concentration. Oxygen fugacity was then related to  $D_V^{\text{olivine/melt}}$  using the empirical calibration  
112 of Wang et al. (2019).

113

## 114 **Results**

115 The average concentrations of V, Al, Ca, Ni, Co, Ga and Y in olivine cores from the studied  
116 OIB samples are listed in **Table 1**. Vanadium concentrations range from  $3.8 \pm 0.4$  (2SD) ppm (in  
117 GC0901) to  $6.3 \pm 0.7$  ppm (in MG1006). Ca concentrations in olivine range from 1017 to 2707  
118 ppm, firmly establishing that the olivines crystallized from magmas and are not mantle  
119 xenocrysts, which are globally characterized by  $<700$  ppm Ca (Foley et al. 2013). Calculated  
120 parental magma compositions, as well as each parental magma's non-bonding  
121 oxygen/tetrahedrally bound oxygen (NBO/T) ratios are listed in **Table 2**. Parental magma MgO  
122 concentrations varied between 8.7 (in PX0802) and 17.4 wt.% (in AVON3-71-22) and parental  
123 magma V concentrations varied between 226 ppm (in PX0802) and 424 ppm (in EH10) while  
124 NBO/T ratios varied between 0.84 (in PX0802) and 1.43 (in AVON3-71-22). All parental lavas had  
125  $>8$  wt.% MgO, and therefore in most cases, olivine was the only accumulated phase, whereas for  
126 a few samples both olivine and clinopyroxene were accumulated phases. To examine whether  
127 clinopyroxene accumulation affected the oxybarometry calculations, we measured the  
128 concentration of V in pyroxene in LP01, EH18 and LZ0601 samples that host large clinopyroxene  
129 crystals. We show that even if the bulk rock contained 50% accumulated pyroxene, the calculated  
130  $fO_2$  would change by 0.27, 0.26, 0.69 log units, respectively. Based on petrographic investigations  
131 (see Online Supplementary Materials), the maximum modal clinopyroxene content is less than

132 30%, and therefore pyroxene accumulation had at most a marginal effect on the calculated  $fO_2$   
133 values. Information on the modeling of clinopyroxene accumulation can be found in **Table 3**.

134 Calculated  $fO_2$  of the OIB samples are listed in **Table 4**, and are relatively uniform, varying  
135 between  $+1.52^{+0.36}_{-0.30}$   $\Delta$ FMQ (in SM0815) and  $+2.86^{+0.28}_{-0.24}$   $\Delta$ FMQ (in GC0901). The four Mangaia  
136 samples all show  $fO_2$  values that overlap within uncertainties of each other, consistent with the  
137 close relationships of lavas in the field and suggesting a statistically identical parental magma.  
138 Calculated  $fO_2$  values for all OIB samples show no correlation with either modeled parental  
139 magma MgO content (**Figure 1**), olivine Mg# (**Supplemental Figure 1**) or bulk rock isotopic  
140 signatures (**Figure 2**), despite wide variation in  $^{206}\text{Pb}/^{204}\text{Pb}$  (from 19.126 to 21.640) and  
141  $^{143}\text{Nd}/^{144}\text{Nd}$  (from 0.512766 to 0.512966). Oxygen fugacity additionally shows no correlation with  
142 parental magma  $\text{Al}_2\text{O}_3$  and  $\text{Na}_2\text{O}$  concentrations (**Tables 2 and 4**), making it unlikely that different  
143 partial melting degrees caused the observed variation. A grand average of all the OIB yields a  
144 value of  $+1.96 \pm 0.70$ , significantly more oxidized than the MORB average using the V-in-olivine  
145 method at  $+0.60 \pm 0.15$   $\Delta$ FMQ (Nicklas et al. 2018) and the MORB average using XANES  
146 measurements at  $-0.18 \pm 0.16$   $\Delta$ FMQ (Zhang et al. 2018) or  $\sim +0.1$   $\Delta$ FMQ (Berry et al. 2018). The  
147 OIB average calculated here is also within uncertainties of data for OIB lavas from Kilauea Iki and  
148 the Western Rift Zone of Iceland of  $+1.64^{+0.19}_{-0.17}$  and  $+1.38^{+0.27}_{-0.23}$   $\Delta$ FMQ, respectively, calculated  
149 using an identical procedure and the olivine and whole rock data of Nicklas et al. (2019). If all the  
150 data are recalculated using higher olivine crystallization temperatures of either 1250°C or 1300°C  
151 (**Table 4**), the relative positions of the data are unaffected and the average shifts to  $+1.63 \pm 0.70$   
152 and  $+1.48 \pm 0.70$   $\Delta$ FMQ, respectively, still significantly higher than MORB.

153

154 **Discussion**

155           Vandium-in-olivine oxybarometry data from this study, combined with those from Hawaii  
156 and Iceland (Nicklas et al., 2019) indicate oxidized mantle sources for all OIB measured to date,  
157 consistent with the conclusions from XANES measurements (Moussallam et al., 2019). Critically,  
158 these observations show that OIB have elevated  $fO_2$  at  $+2.0 \pm 0.7$  (2SD)  $\Delta FMQ$  compared to MORB  
159 at  $+0.6 \pm 0.2$  (2SD)  $\Delta FMQ$ , measured using the same redox proxy, and also lack any correlation  
160 between  $fO_2$  and isotopic signatures or with petrological indicators of magmatic differentiation  
161 (e.g., parental magma MgO, olivine Mg#). A subset of the samples from the Canary Islands,  
162 Mangaia and Samoa have also been analyzed for O and Si stable isotopic systematics (Day et al.  
163 2009; Pringle et al. 2016), but these signatures also show no correlation with  $fO_2$ , although data  
164 are limited. The dichotomy between reduced MORB and oxidized Samoan OIB is also consistent  
165 with the relatively high  $S^{+6}/\Sigma S$  ( $0.17 \pm 0.11$ ) of Samoan lavas (Labidi et al. 2015). The lack of  
166 correlation of  $fO_2$  with isotopic signatures in the OIB dataset contrasts to prior observations made  
167 using MORB datasets. For example, the XANES study of Cottrell and Kelley (2013) showed that  
168 isotopically enriched MORB have resolvable lower  $fO_2$ , which they attributed to reduced carbon  
169 amount in their source regions. This correlation could also possibly instead reflect isotopically  
170 enriched MORB being generally more volatile rich, and thus having degassed more S. Our new  
171 average OIB  $fO_2$  value overlaps with the range of global arc basalts (i.e., Carmichael, 1991; Kelley  
172 and Cottrell, 2009) and also coincides with that of high MgO Siberian meimichites ( $\sim +2.5 \Delta FMQ$ )  
173 estimated using V-in-olivine oxybarometry (Mungall et al. 2005).

174           Although the data of Moussallam et al. (2019) showed that OIB are indeed oxidized, melt  
175 inclusions XANES is perhaps not the best way of constraining OIB source region  $fO_2$  for two main  
176 reasons. Firstly, degassing has affected the measured  $fO_2$  of the samples, and thus only a  
177 minimum  $fO_2$  can be calculated. It has been argued that some modern Canary lavas are the most  
178 S-rich contemporary lavas on Earth and are thus especially susceptible to substantial modification  
179 by degassing (Taracsak et al. 2019). Secondly, several of the samples from that study showed high  
180 volatile concentrations (up to ~3% H<sub>2</sub>O) which can cause significant analytical problems during  
181 XANES analysis (Cottrell et al. 2018) and those authors also did not seek to correlate  $fO_2$  with  
182 isotopic evidence for recycled material in their sample set. The concordance of our average OIB  
183  $fO_2$  with the plume  $fO_2$  inferred by Moussallam et al. (2019) is remarkable, and more V-in-olivine  
184 oxybarometry and XANES measurements of the same samples will serve to clarify the utility of  
185 these two oxybarometry methods for OIB studies.

186

### 187 ***Crustal contamination, degassing and fractional crystallization***

188           The uniformly high  $fO_2$  of OIB strongly suggests that their mantle sources are oxidized  
189 relative to ambient upper mantle sampled by MORB. Oxygen fugacity can be modified, however,  
190 by several post-mantle processes, such as fractional crystallization, crustal contamination, and  
191 degassing of volatiles. Fractional crystallization can oxidize an evolving melt if the fractionating  
192 mineral assemblage preferentially incorporates Fe<sup>+2</sup> over Fe<sup>+3</sup>, as olivine and clinopyroxene do  
193 (Cottrell and Kelley, 2011). Modelling has shown that fractional crystallization has a relatively  
194 minor effect on melt  $fO_2$  until the lava reaches ~8 wt.% MgO (Kelley and Cottrell, 2012), lower

195 than the parental magma compositions of any of the OIB studied here. Additionally, OIB  $fO_2$   
196 shows no correlation with parental magma MgO content (**Figure 1**), indicating negligible effect  
197 of mafic mineral fractionation on  $fO_2$ . More recent studies of MORB lavas show that  $fO_2$  of lavas  
198 can be affected by fractional crystallization (Shorttle et al. 2015) but also found the effect to be  
199 minimal, only increasing  $Fe^{+3}/\Sigma Fe$  by 0.01 per 2.0 wt.% change in MgO content. Given the spread  
200 in parental magma MgO content of the OIB dataset, fractional crystallization will not lead to  
201 significant increases in  $fO_2$ . Due to the generally lower MgO content of MORB lavas (**Figure 1**) and  
202 the fact that crystallization of olivine can only have an oxidizing effect on magma, it is unlikely  
203 that the  $fO_2$  difference between OIB and MORB is generated by fractional crystallization. The  
204 Mangaia samples have radiogenic Pb isotope ratios, and so are likely to contain the largest AOC  
205 contribution yet show among the lowest  $fO_2$  of the OIB samples. The relatively low parental  
206 magma MgO content to the Mangaia samples (10 wt.%) shows that the reported  $fO_2$  would be  
207 even lower if fractional crystallization had significantly affected these samples. We can therefore  
208 rule out significant effects of fractional crystallization on  $fO_2$  for our sample set.

209         Crustal contamination can theoretically oxidize magmas if the assimilated crust is rich in  
210 oxidized elements such as  $Fe^{+3}$ . Due to the relatively low Fe content of the continental crust (and  
211 terrigenous sediments) even ~30% continental crustal assimilation is unlikely to have significantly  
212 affected the  $fO_2$  of a mantle-derived melt (Grocke et al 2005). The studied OIB suites are all  
213 situated on oceanic crust which is relatively Fe-rich, but not grossly more so than the OIB parental  
214 lavas themselves, meaning that significant (>20%) quantities of assimilation would be necessary  
215 to modify their  $fO_2$ . Large amounts of assimilation of oxidized altered oceanic crust from the  
216 underlying plate would affect significantly geochemical signatures of the respective OIB (e.g.,

217 Jackson et al., 2007; Day et al., 2010; Waters et al., 2020), leading to correlations with  $fO_2$ , which  
218 are not observed (**Fig. 3**). In particular, while the available data are limited, no correlation is seen  
219 between O isotopes (Day et al., 2009; 2010) and  $fO_2$ , further demonstrating that assimilation was  
220 a minor process. Finally, although crustal assimilation has been documented in selected Azores  
221 lavas using B and Li isotopes (Genske et al. 2014), such signatures do not indicate the >20%  
222 assimilation necessary to change  $fO_2$  beyond uncertainties.

223 It has been shown in the literature that degassing of sulfur in OIB melts can have a strong  
224 reducing effect on the  $fO_2$  of a melt, with 6 moles of  $Fe^{+3}$  reduced to  $Fe^{+2}$  for every mole of  $S^{-2}$   
225 degassed as  $SO_2$  (Moussallam et al. 2014; 2016; 2019). Water and  $CO_2$  degassing, in contrast,  
226 have negligible effects on the  $fO_2$  of an evolving melt (Moussallam et al. 2014; Waters et al. 2016).  
227 Sulfur degassing is not the cause of the OIB-MORB  $fO_2$  dichotomy for three reasons: first and  
228 most importantly, as V-in-olivine oxybarometry measures  $fO_2$  as olivine is crystallized early in a  
229 magma's evolution, it likely avoids much of the degassing that is observed from XANES  
230 measurements on glass. Second, S degassing has only been shown to have a reducing effect and  
231 could not oxidize OIB relative to MORB, although it is possible that the global MORB signature is  
232 underestimated, as most MORB are sulfide-saturated during eruption (Le Voyer et al. 2015).  
233 Third, our new OIB average overlaps well with the estimate for global undegassed OIB measured  
234 by XANES (Moussallam et al. 2019), which is unlikely if degassing was the root cause of the  
235 oxidized OIB signature. For these reasons, we conclude that the oxidized OIB signature is derived  
236 from a relatively oxidized OIB source mantle, consistent with the conclusions of Moussallam et  
237 al. (2019) and is not the result of later magmatic processes.

238

239 ***Lithologically distinct mantle sources?***

240 It has been postulated that some OIB magmas preferentially sample olivine-free  
241 lithologies such as mantle pyroxenites as opposed to normal mantle peridotite (Sobolev et al.  
242 2005; 2007) due to the high Ni content (and to a lesser extent low Mn and Ca) at constant Mg#  
243 in OIB olivine as opposed to MORB olivine. However, elevated Ni signatures have also been  
244 attributed to contamination by core metal (Herzberg et al. 2013), or high-pressure melting of  
245 normal mantle peridotite (Matzen et al. 2017; Gleeson and Gibson, 2019). To investigate if  
246 different mantle lithologies show different  $fO_2$ , oxygen fugacity is plotted against average olivine  
247 Ni/MgO in **Figure 3**. No correlation is observed, indicating that any difference in  $fO_2$  between  
248 pyroxenite and peridotite in OIB sources is not resolvable in the current dataset. This conclusion  
249 only holds, however, if high Ni in olivine reflects a larger pyroxenite component (Sobolev et al.  
250 2005), which is disputed (Matzen et al. 2017; Gleeson and Gibson, 2019). It is therefore not  
251 simple to determine if OIB lavas originate from melting of peridotite or pyroxenite. For example,  
252 it is also disputed whether the isotopically enriched-endmember in the Canary plume derives  
253 from pyroxenite or peridotite (Day et al. 2009, 2012; Gurenko et al. 2009). Pyroxenite is  
254 conventionally thought to be the result of hybridization of recycled AOC and peridotite (Sobolev  
255 et al. 2005), and therefore would likely be more Fe<sup>+3</sup>-rich (i.e., high  $fO_2$ ) than ambient peridotite.  
256 Either pyroxenite in the sources of the studied OIB is not more oxidized than peridotite, or  
257 pyroxenite-derived melt represents a minor portion of the parental melts contributing to the  
258 studied lavas so as to be undetectable by the method use here. In either scenario, more data are  
259 necessary on pyroxenite and peridotite-derived OIB to clarify the issue. It is worth noting that

260 previous studies have concluded that pyroxenite is lacking in the source of Azores lavas (Sobolev  
261 et al. 2007).

262

### 263 ***Oxidized sources and crustal recycling processes***

264 Oxygen fugacity shows no correlation with bulk-rock isotopic signatures for  $^{206}\text{Pb}/^{204}\text{Pb}$ ,  
265  $^{143}\text{Nd}/^{144}\text{Nd}$  and  $^{187}\text{Os}/^{188}\text{Os}$  (**Figure 2**). This is unexpected, given that the dataset samples a wide  
266 range of geochemical compositions, including some of the most extreme HIMU signatures  
267 present in mantle-derived lavas, which are likely to host large amounts of AOC in their source  
268 regions. The Mangaia HIMU end-member likely hosts a component of subducted  $\sim 2.5$  Ga AOC  
269 (e.g., Cabral et al., 2013). HIMU is characterized by high  $^{206}\text{Pb}/^{204}\text{Pb}$ , which results from high  
270  $^{238}\text{U}/^{204}\text{Pb}$  in a long-lived mantle source (Chauvel et al. 1992; Woodhead et al. 1996). The mantle  
271 source of HIMU lavas is thought to host  $\sim 5\%$  AOC mixed with ambient mantle (Nebel et al. 2013).  
272 Whether the AOC is present as a separate, oxidized pyroxenite lithology or the isotopic signatures  
273 of AOC have been imparted onto normal peridotite without a separate lithology being present is  
274 unsettled (Herzberg et al. 2014).

275 For the purpose of our modeling, we assume that AOC isotopic signatures in the Mangaia  
276 source are accompanied by oxidized AOC Fe. AOC has a relatively high  $\text{Fe}^{+3}/\Sigma\text{Fe}$  of  $0.22 \pm 0.08$  but  
277 can locally reach values as high as 0.36 (Evans, 2012). Even Archean AOC is likely highly oxidized,  
278 as oxidation of AOC is largely the result of serpentinization reactions in the presence of water  
279 and has little to do with atmospheric  $\text{O}_2$  content (i.e., Kasting, 2014). Assuming that ambient  
280 MORB mantle has 8.05 wt.% total FeO (McDonough and Sun, 1995) with a  $\text{Fe}^{+3}/\Sigma\text{Fe} = 0.05$

281 (Cottrell and Kelley, 2011) and recycled AOC has 10.43 wt.% total FeO (Gale et al. 2013) with a  
282  $\text{Fe}^{+3}/\Sigma\text{Fe} = 0.22$  to 0.36 (Evans, 2012), a mixture of 95% ambient mantle and 5% AOC has a  
283  $\text{Fe}^{+3}/\Sigma\text{Fe}$  of 0.06 to 0.07. Assuming temperature is constant and mantle spinel does not change  
284 in composition by addition of AOC except to increase in  $\text{Fe}^{+3}$  content, addition of 5% AOC is  
285 calculated using the method of Ballhaus et al. (1991) to raise the  $f\text{O}_2$  of the HIMU source by 0.34-  
286 0.58 log units  $\Delta\text{FMQ}$ . These differences are possibly resolvable using our method, which has  
287 uncertainties varying from 0.13 to 0.59 log units  $\Delta\text{FMQ}$ .

288         The reason for the uniform OIB  $f\text{O}_2$  signature can perhaps be attributed to the differing  
289 compatibilities of lithophile trace element systems and redox-sensitive elements. By far the most  
290 abundant redox-sensitive element in mantle and recycled crustal lithologies is Fe (Evans, 2012),  
291 which is a major element in both mantle and crust and shows only a moderate degree of  
292 incompatibility during melting events. By contrast, parent, daughter or both isotopes in the Rb-  
293 Sr, Sm-Nd, U-Pb, Th-Pb and Lu-Hf systems, all consist of highly incompatible elements.  
294 Abundances of Sr, Nd, Pb, and Hf are all highly enriched in crustal lithologies relative to the  
295 depleted mantle (Rudnick and Gao, 2003; Salters and Stracke, 2004), and therefore their budget  
296 in OIB lavas may be dominated by a volumetrically minor enriched lithology similar to the model  
297 of Stracke et al. (2019). For example, extreme EM2 lavas from Samoa show strong isotopic  
298 similarities to continental sediments, but the signature can be explained by mixing only ~6%  
299 sediment into their mantle source region (Jackson et al. 2007). Indeed, Samoan lavas studied  
300 here show average  $f\text{O}_2$  that is not resolvable from the global OIB dataset.

301           The radiogenic components responsible for HIMU may not mix as a separate lithology  
302 with ambient mantle, but instead melt and mix with melts derived from more depleted mantle  
303 lithologies. The chalcophile nature of Pb (Hart and Gaetani, 2006) during mantle melting means  
304 that a very small volume of S-rich melt could host radiogenic Pb, dampening such a melt's effect  
305 on  $fO_2$  and major element abundances. Strong variations in OIB isotopic signatures are generally  
306 only present for elements that are highly enriched in crustal lithologies, as demonstrated by the  
307 relatively muted variations in major element isotopic signatures in OIB, such as Fe and Si isotopes  
308 (Williams et al. 2014; Pringle et al. 2016). Notably, Os is highly compatible during mantle melting,  
309 and Os isotope systematics are often decoupled from lithophile isotope systems in OIB as  
310 peridotite components will control Os systematics while recycled components control lithophile  
311 isotope systematics (Day 2013). Lead isotopic signatures are also decoupled from Nd, Sr, and Hf  
312 isotopic systematics, likely because Pb is controlled by mantle sulfide as opposed to silicate  
313 phases (Hart and Gaetani, 2006). The high  $fO_2$  component in OIB therefore probably samples a  
314 common, volumetrically dominant plume component (i.e., depleted plume or ambient mantle  
315 component) relative to the volumetrically minor recycled components that are enriched in  
316 incompatible elements that control Nd, Sr, Hf and potentially Pb isotope systematics. This simple  
317 conceptual model leads to the lack of correlation between oxygen fugacity and long-lived  
318 radiogenic or stable isotope systematics.

319

320 ***Oxidation processes in OIB mantle sources***

321           Although isotopic parameters show no systematic variations with oxygen fugacity  
322 between OIB samples, it is evident that the OIB probe more isotopically enriched and diverse  
323 mantle signatures and are more oxidized than MORB. The presented dataset can be used to  
324 constrain the isotopic composition of this mantle component present in OIB but not MORB.  
325 Numerous studies have proposed the existence of a common mantle component present in OIB  
326 (e.g., Hart et al. 1992; Farley et al. 1992; Stracke et al. 2005), which has been termed either  
327 “FOZO” or “PHEM”. This component is thought to be located at the intersection of all major OIB  
328 isotopic arrays and to carry a high- $^3\text{He}/^4\text{He}$  ratio and moderately depleted Sr, Nd, and Hf isotopic  
329 signatures and unradiogenic Pb. If this component is indeed present in all the studied OIB  
330 samples, it may be volumetrically dominant enough to give all the OIB uniformly elevated  $f\text{O}_2$ .  
331 Selected Samoan lavas examined here have been shown to have high  $^3\text{He}/^4\text{He}$  (Ofu-04-14 has  
332  $^3\text{He}/^4\text{He}$  of 25  $R_a$ ; Jackson et al. 2007b), but Canary Islands (Day & Hilton, 2011), and Mangaia  
333 lavas have lower  $^3\text{He}/^4\text{He}$ , in some cases even lower than MORB lavas (Parai et al., 2009). Azores  
334 lavas are largely MORB-like with regard to He isotopes, ranging from 7.2 to 11.1  $R_a$  (Moriera et  
335 al. 1999; 2012; Madureira et al. 2014). It is notable that regardless of the wide variation in He  
336 isotopic signatures in the studied OIB, there seems to be no variation in their  $f\text{O}_2$ .

337           If the “common” component sampled by OIB is more oxidized relative to the MORB  
338 source mantle, then a model explaining its high  $f\text{O}_2$  is necessary. If the common component is  
339 simply a constant amount of relatively young, recycled AOC, as suggested by Stracke et al. (2005),  
340 this could be a potential source of the MORB-OIB  $f\text{O}_2$  dichotomy, but this model does not explain  
341 the high- $^3\text{He}/^4\text{He}$  signature seen in Samoan OIB, as recycled crust is predicted to have low-  
342  $^3\text{He}/^4\text{He}$ . Alternatively, if the high- $^3\text{He}/^4\text{He}$  common component is an early, less degassed

343 primordial reservoir (Class and Goldstein, 2005), its high  $fO_2$  may reflect a more oxidized  
344 signature for such a reservoir. The DMM likely lost some of its oxidized elements by melting  
345 events depleting it in  $Fe^{+3}$  over time while the common component could have remained  
346 relatively undepleted. More extensive modeling on the effect of melting on the  $fO_2$  of residual  
347 mantle lithologies is needed to constrain this model. Alternatively, if the common component is  
348 hosted in the lower mantle, and formed early in Earth history, it could be oxidized due to the loss  
349 of disproportionated metallic Fe (i.e., metallic Fe formed from the reaction  $3Fe^{+2} \rightarrow Fe^0 + 2Fe^{+3}$ )  
350 from the lowermost mantle during a primordial magma ocean phase (Wood et al. 2006). If the  
351 common component was oxidized shortly after core formation and preserved (unmixed with  
352 upper mantle) until the present day, it would present an oxidized signature, similar to the model  
353 for the source of the 3.55 Ga Schapenburg komatiites (Nicklas et al. 2019). The Schapenburg  
354 komatiites show isotopic evidence for early lower mantle processes as well as very high  $fO_2$   
355 compared to other Archean komatiites, making it likely that their mantle source region was  
356 oxidized by loss of disproportionated Fe early in Earth history. While it may seem implausible that  
357 early-formed mantle reservoirs could still be sampled by modern plume lavas, the high- $^3He/^4He$   
358 signatures of OIB and the recently discovered  $^{182}W/^{184}W$  anomalies in OIB with high- $^3He/^4He$   
359 (Mundl et al., 2017) suggest that primordial mantle signatures continue to be sampled in modern  
360 lavas. Regardless of whether the high  $fO_2$  of the common OIB component is the result of a  
361 uniform recycled source (Stracke et al., 2005) or an early-formed geochemically depleted source  
362 (Hart et al., 1992; Mundl-Petermeier et al., 2020), more OIB  $fO_2$  data from more plumes, including  
363 those with extreme isotopic signatures, are necessary to clarify the issue. Of particular interest is  
364 the measurement of  $fO_2$  in samples with  $^{182}W/^{184}W$  anomalies, which are sensitive indicators of

365 the presence of early-formed components in mantle plume sources. The current dataset only  
366 includes one such sample, OFU-4-14, that shows a strongly negative  $\mu^{182}\text{W}$  anomaly of  $-17.3 \pm$   
367  $4.5$  (Mundl-Petermeier et al. 2020) and  $^3\text{He}/^4\text{He}$  ratio of 25 Ra (Jackson et al. 2007) but close to  
368 average OIB  $f\text{O}_2$  of  $+1.78^{+0.25}_{-0.22} \Delta\text{FMQ}$ .

369 Our new  $f\text{O}_2$  data support the paradigm that recycled surficial materials such as AOC and  
370 sediments are present in the sources of OIB (Hofmann, 1997), possibly leading to their high  $f\text{O}_2$   
371 value. There is a strong theoretical framework to support this idea, as mass-balance calculations  
372 in subduction zones (Evans, 2012; Brounce et al. 2019) show that the majority of contemporary  
373 subducted oxidants ( $\text{Fe}^{+3}$ ,  $\text{S}^{+8}$ ,  $\text{C}^{+4}$ ) are not emitted by arc volcanoes, indicating that they are  
374 brought into the deep mantle. Indeed, the global study of Evans (2012) suggested that only  $\sim 10\%$   
375 of the total subducted oxidants, and almost none of the subducted  $\text{Fe}^{+3}$ , is emitted by global arc  
376 volcanoes. There is substantial isotopic variation found in OIB (Zindler and Hart, 1984; Hofmann,  
377 1997) likely because of varying proportions of recycled AOC, as well as terrigenous and pelagic  
378 sediments. These different lithologies are likely to show substantially different oxygen fugacity,  
379 with AOC and terrigenous sediment being oxidized relative to the mantle, and pelagic organic-  
380 rich sediments being reduced. This study shows that the quantity and type of recycled material  
381 does not appear to impact the  $f\text{O}_2$  of the lava. Prior to this study, no work has attempted to  
382 correlate isotopic signatures of OIB with oxygen fugacity. More data will show whether the OIB  
383 source mantle is indeed uniformly more oxidized than MORB and whether any variation is shown  
384 with isotopic signatures.

385

386 **Conclusions**

387 In order to investigate the putatively high oxygen fugacity of the mantle source regions  
388 of plume lavas relative to the depleted MORB mantle, we measured the trace element  
389 systematics of primitive olivine phenocrysts from twenty OIB samples from the Azores, Samoa,  
390 the Canary Islands and the Cook Islands. The OIB samples show a wide range of isotopic  
391 signatures, likely sampling a wide variety of recycled crustal materials. Olivine trace element  
392 systematics was used to constrain magmatic  $fO_2$  in each sample using the V-in-olivine  
393 oxybarometry method. All OIB samples are similar in  $fO_2$ , ranging from  $+1.52^{+0.36}_{-0.30}$   $\Delta$ FMQ to  
394  $+2.86^{+0.28}_{-0.24}$   $\Delta$ FMQ, with an average of  $1.96 \pm 0.70$   $\Delta$ FMQ, significantly more oxidized than the  
395 V-in-olivine oxybarometry MORB average of  $+0.60 \pm 0.15$   $\Delta$ FMQ. Additionally, OIB  $fO_2$  shows no  
396 correlation with whole rock  $^{206}\text{Pb}/^{204}\text{Pb}$ ,  $^{143}\text{Nd}/^{144}\text{Nd}$  and  $^{187}\text{Os}/^{188}\text{Os}$  ratios, or with parental  
397 magma MgO or inferred pyroxenite content in their source regions. Given the probable presence  
398 of oxidized altered oceanic crust in high  $^{206}\text{Pb}/^{204}\text{Pb}$  OIB, such a null result is significant. This is  
399 likely due to isotopic signatures being dominated by volumetrically small, trace element-enriched  
400 components, while  $fO_2$  reflects the volumetrically dominant component of the OIB source region.  
401 The large and consistent gap in  $fO_2$  between MORB and OIB samples indicates that the  
402 volumetrically dominant plume component was oxidized relative to the depleted mantle. Two  
403 main mechanisms can explain this: either the net OIB source mantle has uniformly high amounts  
404 of recycled oceanic crust, or the OIB source reflects a primitive undegassed oxidized reservoir.  
405 Early mantle material could have become oxidized shortly after core formation by the  
406 segregation of disproportionated Fe metal formed in the lower mantle and be preserved unmixed  
407 in the lower mantle till the present day. The presence of  $^{182}\text{W}/^{184}\text{W}$  isotope anomalies in modern

408 OIB lend credence to the idea that plumes may sample early formed mantle reservoirs. The new  
409 dataset presented here confirms that the modern mantle is heterogeneous with respect to  $fO_2$   
410 and that different mantle reservoirs can be accurately characterized using the V-in-olivine  
411 oxybarometry method in the future.

412

### 413 **Acknowledgements**

414 Funding for this project was provided by National Science Foundation EAR Grant  
415 #1918322 “A mixed-up mantle beneath Ocean Islands?” (to JMDD). We are grateful to J. Lyakov  
416 for development of the LA-ICP-MS correction program. Comments by Oliver Shorttle and an  
417 anonymous reviewer are gratefully acknowledged.

418

### 419 **Author Contributions:**

420 RWN and JMDD designed the project. RKMH and RWN prepared and performed the  
421 analyses, data reduction and calculations. The manuscript was written by RWN and RKMH with  
422 editing from JMDD, MGJ, VZ, RA and LNW. Samples were collected by JMDD, VZ and MGJ. JMDD  
423 provided funding and technical support for the project.

**Figure Captions**

**Figure 1.** Calculated  $fO_2$  of the OIB samples plotted against MgO content of parental magmas. MORB  $fO_2$  field based on olivine-glass pairs from Nicklas et al. (2019).

**Figure 2a.** Calculated  $fO_2$  of the OIB samples plotted against bulk rock  $^{187}\text{Os}/^{188}\text{Os}$  ratios. **b.** Calculated  $fO_2$  of the OIB samples plotted against bulk rock  $^{206}\text{Pb}/^{204}\text{Pb}$  ratios. **c.** Calculated  $fO_2$  of the OIB samples plotted against bulk rock  $^{143}\text{Nd}/^{144}\text{Nd}$  ratios. Sources of isotope data are listed in **Table 4**. MORB isotopic data are from Workman and Hart (2005) and MORB  $fO_2$  data are from Nicklas et al. (2018). Symbols as in **Fig. 1**.

**Figure 3.** Average Ni/MgO, in ppm/wt. % of olivine plotted against calculated  $fO_2$  for each suite. Symbols as in **Fig. 1**.

**Table 1:** Average concentrations of elements (in ppm) in the cores of primitive olivine crystals from each OIB sample. Data were reduced assuming uniform Si concentrations, which are taken from the literature, and vary the least of all major elements in stoichiometric olivine. *N* – number of olivine grains analyzed for each sample, SiO<sub>2</sub> – assumed silica content of the olivine in wt.%, 2s – two standard deviations of the average concentration. For full dataset including concentrations in each spot analyzed, see online supplemental datasets.

Sample	N	SiO <sub>2</sub>	Al	Ca	V	Co	Ni	Ga	Y
LP03	19	39.28	161.4	1677	4.88	160.3	1503		
2s			34.5	518	0.77	34.7	318		
EH10	20	38.91	182.7	1473	5.77	212.7	1369	0.20	0.14
2s			39.7	259	1.11	17.4	599	0.03	0.05
GOM05	23	39.70	238.5	1774	6.21	180.9	1669	0.19	0.13
2s			76.2	265	1.16	14.0	177	0.06	0.04
LZ0601	25	38.99	232.7	1756	6.16	180.4	1653	0.19	0.13
2s			84.5	283	1.26	14.0	202	0.06	0.04
GC0901	19	39.05	161.4	1871	3.80	179.5	2044	0.17	0.14
2s			22.3	208	0.43	11.7	192	0.04	0.04
EH18	24	38.98	160.2	1017	5.79	198.6	1539	0.19	0.14
2s			40.1	280	1.03	29.2	1186	0.04	0.08
LP01	33	39.05	170.6	1712	5.27	193.1	1289	0.16	0.13
2s			58.8	388	1.07	20.2	165	0.05	0.05
9CTEN05	20	39.63	203.2	2111	4.87	187.0	1476	0.16	0.12
2s			27.1	249	0.53	18.4	313	0.02	0.03
04PAL05	20	39.39	201.6	2157	4.03	157.1	1785	0.14	0.11
2s			47.9	273	0.44	11.6	163	0.03	0.02
MG01	24	39.29	204.3	2575	5.63	187.1	1481	0.15	0.14
2s			20.3	204	0.60	10.1	66	0.03	0.02
MG02	23	38.79	202.4	2707	5.26	187.5	1523	0.11	0.15
2s			16.5	242	0.47	13.7	107	0.14	0.03
MG06	23	39.36	216.8	2340	6.34	225.1	1207	0.13	0.18
2s			42.7	363	0.65	13.1	176	0.16	0.02
MG08	23	39.15	215.7	2115	6.28	206.1	1203	0.12	0.15
2s			23.2	312	0.91	19.1	300	0.18	0.03
SM0815	19	39.75	267.4	1968	5.42	179.2	1334	0.18	0.12
2s			90.4	508	0.89	34.4	611	0.03	0.03
PX0802	25	39.14	192.7	1389	5.51	161.9	1307	0.17	0.14
2s			40.7	374	0.79	17.1	348	0.04	0.07
TR0802	26	39.21	311.8	1805	5.09	137.2	1949	0.20	0.11
2s			174.0	422	1.31	38.0	1146	0.11	0.05
T-25	19	39.54	199.3	2061	5.59	161.1	2079	0.15	0.12
2s			30.9	430	0.80	26.8	287	0.11	0.07
OFU04-14	20	39.61	184.5	1882	5.74	185.2	1681	0.18	0.11

2s			26.7	469	0.55	33.3	125	0.03	0.04
AVON2-62-2	20	40.34	314.2	2187	4.95	159.1	2340	0.19	0.12
2s			133.1	943	1.16	30.5	653	0.05	0.04
AVON3-71-2	20	40.38	208.0	2273	5.00	156.8	1923	0.14	0.11
2s			75.5	460	0.99	15.0	493	0.05	0.03

**Table 2:** Calculated major element compositions in weight %, and V concentration in ppm of parental magmas of the studied OIB samples. NBO/T is the ratio of non-bonding oxygens to tetrahedrally bonded oxygens in the parental magmas, calculated using the procedure of Mills (1993).

Sample	SiO <sub>2</sub>	TiO <sub>2</sub>	Al <sub>2</sub> O <sub>3</sub>	FeO	MnO	MgO	CaO	Na <sub>2</sub> O	K <sub>2</sub> O	P <sub>2</sub> O <sub>5</sub>	V (ppm)	NBO/T
LP03	51.3	2.90	11.2	13.0	0.22	12.0	8.34	0.50	0.11	0.39	266	0.95
EH10	41.2	5.92	10.6	16.0	0.21	10.7	11.3	2.52	0.85	0.76	424	1.31
GOM05	46.0	3.21	11.0	12.5	0.19	13.3	9.27	2.94	0.84	0.69	296	1.20
LZ0601	47.0	2.68	13.3	13.0	0.17	9.48	11.2	1.86	0.90	0.42	292	0.97
GC0901	44.4	4.83	13.0	12.0	0.18	9.14	12.2	2.80	1.00	0.44	354	1.02
EH18	43.5	5.59	11.7	13.8	0.21	9.85	10.4	3.28	1.02	0.67	368	1.11
LP01	46.1	3.59	11.6	12.3	0.20	9.86	12.8	2.33	0.87	0.44	368	1.11
9CTEN05	45.5	2.59	10.6	12.1	0.17	13.14	12.9	2.03	0.62	0.31	282	1.32
04PAL05	42.8	3.40	11.6	12.9	0.18	11.69	13.5	2.47	0.84	0.63	402	1.30
Mangaia	44.9	2.83	11.7	12.9	0.19	10.0	14.3	2.20	0.62	0.39	311	1.20
SM0815	47.5	3.00	12.2	10.7	0.16	12.6	8.94	2.62	1.96	0.43	243	1.06
PX0802	48.7	2.52	14.2	9.91	0.17	8.66	10.5	3.48	1.30	0.48	226	0.84
TR0802	47.9	2.70	14.1	10.0	0.16	9.00	12.21	2.65	0.90	0.51	262	0.89
T-25	46.8	3.06	10.5	12.9	0.19	13.2	10.3	2.00	0.79	0.35	339	1.23
OFU04-14	46.0	3.89	8.88	13.2	0.17	13.1	12.3	1.53	0.62	0.35	339	1.36
AVON2-62-2	48.2	1.99	9.02	10.3	0.17	17.3	10.5	1.58	0.70	0.22	262	1.40
AVON3-71-22	47.5	1.90	9.22	10.0	0.18	17.4	11.1	1.58	0.73	0.22	270	1.43

**Table 3:** Average clinopyroxene V concentrations as determined by a LA-ICP-MS procedure identical to the one for olivine. Bulk rock V concentrations used to determine  $fO_2$  is also listed, along with a bulk V concentration from which 5%, 10%, 20%, 40% and 50% of the measured clinopyroxene removed. Finally, the calculated  $fO_2$  for each sample is listed, along with an  $fO_2$  calculated using the bulk rock compositions with varying amounts of clinopyroxene removed. As demonstrated by the modeling shown here, clinopyroxene accumulation has a negligible effect on the calculated  $fO_2$  unless extremely large amount of clinopyroxene was accumulated in the bulk rock samples. *CPX* – clinopyroxene, *2s* – two standard deviations, *N* – number of clinopyroxenes analyzed.

<b>Sample</b>	<b>LP01</b>	<b>EH18</b>	<b>LZ0601</b>
<b>CPX V (ppm)</b>	270	294	326
<b>2s</b>	40	55	101
<b>N</b>	9	12	10
<b>Bulk V (ppm)</b>	328	357	242
<b>Without 5% CPX</b>	331	360	238
<b>Without 10% CPX</b>	335	364	233
<b>Without 20% CPX</b>	343	372	221
<b>Without 30% CPX</b>	353	383	206
<b>Without 40% CPX</b>	367	398	186
<b>Without 50% CPX</b>	386	419	158
<b><math>fO_2</math> (<math>\Delta FMQ</math>)</b>	2.30	2.14	1.77
<b>Without 5% CPX</b>	2.31	2.15	1.73
<b>Without 10% CPX</b>	2.33	2.17	1.69
<b>Without 20% CPX</b>	2.37	2.21	1.61
<b>Without 30% CPX</b>	2.42	2.26	1.49
<b>Without 40% CPX</b>	2.49	2.32	1.31
<b>Without 50% CPX</b>	2.57	2.41	1.04

**Table 4:** Calculated parental magma  $fO_2$ , in log units relative to the FMQ buffer, as well as bulk rock isotope ratios for the studied OIB samples. The preferred values at 1150°C for oxygen fugacity are listed under “FMQ” but also listed are oxygen fugacity values calculated using different olivine crystallization temperatures of 1250°C and 1300° demonstrating the lack of a strong temperature effect on the results. Up – positive uncertainty on the calculated  $fO_2$ , down – negative uncertainty on the calculated  $fO_2$ . 2s – quoted 2 sigma uncertainties on the isotope ratios. Sources of isotope data: Jackson et al. (2007a); Day et al. (2010); Jackson et al. (2014); Waters et al. (2020); Day et al. (under review) and Day (unpublished data).

Sample	Location	MgO	FMQ	Up	Down	$^{206}\text{Pb}/^{204}\text{Pb}$	2s	$^{143}\text{Nd}/^{144}\text{Nd}$	2s	$^{187}\text{Os}/^{188}\text{Os}$	2s	FMQ at 1250C	FMQ at 1300C
LP03	La Palma	12.01	2.02	0.35	0.29	19.698	0.007	0.512966	0.000017	0.14406	0.00001	1.69	1.54
EH10	El Hierro	10.69	2.20	0.41	0.33	19.597	0.007	0.512942	0.000003	0.14808	0.00005	1.87	1.72
GOM05	La Gomera	13.32	1.93	0.27	0.23	-	-	-	-	-	-	1.59	1.44
LZ0601	Lanzarote	9.48	1.77	0.43	0.34	-	-	-	-	-	-	1.44	1.29
GC0901	Gran Canaria	9.14	2.86	0.28	0.24	-	-	-	-	-	-	2.53	2.38
EH18	El Hierro	9.85	2.14	0.38	0.31	19.666	0.001	0.512952	0.000005	0.15297	0.00006	1.80	1.65
LP01	La Palma	9.86	2.30	0.43	0.34	19.759	0.001	0.512914	0.000004	0.14328	0.00001	1.96	1.81
9CTEN05	Tenerife	13.14	1.79	0.27	0.23	-	-	-	-	-	-	1.45	1.30
04PAL05	La Palma	11.69	2.71	0.27	0.23	-	-	-	-	-	-	2.38	2.23
MG01	Mangaia	10.03	1.74	0.19	0.17	21.601	0.002	0.512919	0.000005	0.14982	0.00008	1.41	1.26
MG02	Mangaia	10.03	1.78	0.16	0.15	21.600	0.002	0.512914	0.000006	0.16064	0.00009	1.45	1.30
MG06	Mangaia	10.03	1.67	0.19	0.16	21.640	0.002	0.512907	0.000007	0.16600	0.00010	1.34	1.19
MG08	Mangaia	10.03	1.78	0.26	0.23	21.630	0.002	0.512904	0.000008	0.15243	0.00006	1.45	1.30
SM0815	Sao Miguel	12.55	1.52	0.36	0.30	19.889	0.0002	0.512736	0.000003	-	-	1.19	1.04
PX0802	Pico	8.66	1.65	0.32	0.27	19.804	0.0003	0.512884	0.000003	0.12460	0.00130	1.32	1.17
TR0802	Terceira	9.00	1.99	0.54	0.41	19.311	0.0003	0.512938	0.000003	0.13840	0.00272	1.66	1.51
T-25	Ta'u	13.17	1.95	0.32	0.27	19.2266	0.0007	0.512790	0.000040	0.12334	0.00009	1.62	1.47
OFU04-14	Ofu	13.12	1.78	0.25	0.22	19.1260	0.00003	0.512819	0.000025	0.12947	0.00008	1.45	1.30
AVON2-62-2	Vailulu'u	17.44	1.56	0.49	0.38	-	-	-	-	0.12826	0.00004	1.23	1.08
AVON3-71-22	Vailulu'u	17.31	2.03	0.42	0.34	19.358	0.0002	0.512747	0.000040	0.12762	0.00007	1.70	1.55

**Works Cited:**

- Ballhaus, C., Berry, R. F., Green, D. H. (1991). High pressure experimental calibration of the olivine-orthopyroxene-spinel oxygen geobarometer: implications for the oxidation state of the upper mantle. *Contrib. Mineral. Petrol.* **107**: 27-40.
- Berry A. J., Stewart G. A., O'Neill H. St. C., Mallmann G., Mosselmans J. F. W. (2018) A re-assessment of the oxidation state of iron in MORB glasses. *Earth and Planetary Science Letters* **483**: 114-123.
- Brounce, M. N., Cottrell, E., Kelley, K. A. (2019). The Redox Budget of the Marianas Subduction Zone. *Earth and Planetary Science Letters* **528**: 115859.
- Brounce M. N., Stolper E., Eiler, J. (2017) Redox variations in Mauna Kea lavas, the oxygen fugacity of the Hawaiian plume, and the role of volcanic gases in Earth's oxygenation. *Proc. Natl. Acad. Sci.* **114**, 8997–9002.
- Brounce M. N., Kelley K. A., Cottrell E. (2014) Variations in  $\text{Fe}^{+3}/\Sigma\text{Fe}$  of Mariana Arc Basalts and Mantle Wedge  $\text{fO}_2$ . *J. Petrol.* **55**, 2513–2536.
- Cabral, R. A., Jackson, M. G., Rose-Koga, E. F., Koga, K. T., Whitehouse, M. J., Antonelli, M. A., Farquhar, J., Day, J. M. D., Hauri, E. H. (2013) Anomalous sulphur isotopes in plume lavas reveal deep mantle storage of Archaean crust. *Nature* **496**: 490-493.
- Canil D. (1997) Vanadium partitioning and the oxidation state of Archaean komatiite magmas. *Nature* **389**, 842–845.
- Carmichael I. S. (1991) The redox states of basic and silicic magmas: A reflection of their source regions? *Contrib. Mineral. Petrol.* **106**, 129–141.
- Chakraborty, S. (2010) Diffusion coefficients in Olivine, Wadleysite and Ringwoodite. *Reviews in Mineralogy and Geochemistry* **72**: 603-639.
- Chauvel C., Hofmann A. W., Vidal P. (1992) HIMU-EM: The French Polynesian connection. *Earth and Planetary Science Letters* **110**: 99-119.
- Class C., Goldstein S. L. (2005) Evolution of helium isotopes in the Earth's mantle. *Nature* **436**: 1107-1112.
- Cottrell E., Lanzirotti A., Mysen B., Birner S., Kelley K. A., Botcharnikov R., Davis F. A., Newville M. (2018) A Mössbauer-based XANES calibration for hydrous basalt glasses reveals radiation-induced oxidation of Fe. *American Mineralogist* **103**: 489-501.
- Cottrell E., Kelley K. A. (2013) Redox Heterogeneity in Mid-Ocean Ridge Basalts as a Function of Mantle Source. *Science* **340**(6138): 1314-1317.

- Cottrell E. Kelley K. A. (2011) The oxidation state of Fe in MORB glasses and the oxygen fugacity of the upper mantle. *Earth Planet. Sci. Lett.* **305**, 270–282.
- Day J. M. D., Walker R. J., Watanabe S., Hanski E., Jackson M. G., Widom E. (2020) Osmium-186 anomalies in ocean island basalts from early Earth differentiation. *Science Advances* (under review)
- Day J. M. D. (2013) Hotspot volcanism and highly siderophile elements. *Chemical Geology* **341**: 50-74.
- Day J. M. D., Hilton D. R. (2011) Origin of  $^3\text{He}/^4\text{He}$  ratios in HIMU-type basalts constrained from Canary Island lavas. *Earth and Planetary Science Letters* **305**: 226-234.
- Day J. M. D., Pearson D. G., Macpherson C. G., Lowry D., Carracedo J.-C. (2010) Evidence for distinct proportions of subducted oceanic crust and lithosphere in HIMU-type mantle beneath El Hierro and La Palma, Canary Islands. *Geochimica et Cosmochimica Acta* **74**: 6565-6589.
- Day J. M. D., Pearson D. G., Macpherson C. G., Lowry D., Carracedo J.-C. (2009) Pyroxenite-rich mantle formed by recycled oceanic lithosphere: Oxygen-osmium isotope evidence from Canary Island lavas. *Geology* **37**(6): 555-558.
- Evans K. A. (2012) The redox budget of subduction zones. *Earth-Sci. Rev.* **113**, 11–32.
- Farley K. A., Natland J. H., Craig H. (1992) Binary mixing of enriched and undegassed (primitive?) mantle components (He, Sr, Nd, Pb) in Samoan lavas. *Earth and Planetary Science Letters* **111**: 183-199.
- Foley S. F., Prelevic D., Rehfeldt T., Jacob D. E. (2013) Minor and trace elements in olivine as probes into early igneous and mantle melting processes. *Earth and Planetary Letters* **363**: 181-191.
- Gale A., Dalton C. A., Langmuir C. H., Su Y., Schilling J.-G. (2013) The mean composition of ocean ridge basalts. *Geochemistry, Geophysics, Geosystems* **14**(3): 489-518.
- Genske F. S., Turner S. P., Beier C., Chu M.-F., Tonarini S., Pearson N. J., Haase K. M. (2014) Lithium and boron isotope systematics in lavas from the Azores islands reveal crustal assimilation. *Chemical Geology* **373**: 27-36.
- Gleeson M. L. M., Gibson S. A. (2019) Crustal controls on apparent mantle pyroxenite signals in ocean-island basalts. *Geology* **47**(4): 321-324.
- Grocke S. B., Cottrell E., Silva S. D. and Kelley K. A. (2016) The role of crustal and eruptive processes versus source variations in controlling the oxidation state of iron in Central Andean magmas. *Earth Planet. Sci. Lett.* **440**, 92–104.

- Gurenko A. A., Sobolev A. V., Hoernle K. A., Hauff F., Schmincke H.-U. (2009) Enriched, HIMU-type peridotite and depleted recycled pyroxenite in the Canary plume: A mixed-up mantle. *Earth and Planetary Science Letters* **277**: 514-524.
- Hart, S. R., Gaetani, G. A. (2006). Mantle Pb paradoxes: the sulfide solution. *Contrib. Mineral. Petrol.* **152**: 295-308.
- Hart, S. R., Hauri, E. H., Oschmann, L. A., Whitehead, J. A. (1992). Mantle Plumes and Entrainment: Isotopic Evidence. *Science* **256**: 517-520.
- Helz R. T., Cottrell E., Brounce M. N., Kelley K. A. (2017). Olivine-melt relationships and syneruptive redox variations in the 1959 eruption of Kīlauea Volcano as revealed by XANES. *Journal of Volcanology and Geothermal Research* **333-334**: 1-14.
- Herzberg C., Cabral C. A., Jackson M. G., Vidito C., Day J. M. D., Hauri E. H. (2014). Phantom Archean crust in Mangaia Hotspot Lavas and the meaning of heterogeneous mantle. *Earth and Planetary Science Letters* **396**: 97-106.
- Herzberg C., Asimow P. D., Ionov D. A., Vidito C., Jackson M. G., Geist D. (2013). Nickel and helium evidence for melt above the core-mantle boundary. *Nature* **493**: 393-397.
- Hofmann A. W. (1997). Mantle geochemistry: the message from oceanic volcanism. *Nature* **385**: 219-229.
- Jackson, M.G. Hart S. R., Konter, J. G., Kurz, M. D., Blusztajn, J., Farley, K. A. (2014). Helium and lead isotopes reveal the geochemical geometry of the Samoan plume. *Nature* **514**: 355-358.
- Jackson M. G., Hart S. R., Koppers A. A. P., Staudigel H., Konter J., Blusztajn J., Kurz M., Russell J. A. (2007) The return of subducted continental crust in Samoan lavas. *Nature* **448**: 684-687.
- Kasting J. (2014) Mantle Cooling, Seafloor Serpentinization, and the Rise of Atmospheric O<sub>2</sub>. American Geophysical Union Fall Meeting, Abstract #P11C-3782.
- Kelley K. A. and Cottrell E. (2012) The influence of magmatic differentiation on the oxidation state of Fe in a basaltic arc magma. *Earth Planet. Sci. Lett.* **329-330**, 109–121.
- Kelley K. A. and Cottrell E. (2009) Water and the Oxidation State of Subduction Zone Magmas. *Science* **325**: 605-607.
- Kress V. C. and Carmichael I. S. E. (1991) The compressibility of silicate liquidus containing Fe<sub>2</sub>O<sub>3</sub> and the effect of composition, temperature, oxygen fugacity and pressure on their redox states. *Contrib. Mineral. Petrol.* **103**, 82–92.

- Labidi J., Cartigny, P. Jackson M. G. (2015). Multiple sulfur isotope composition of oxidized Samoan melts and the implications of a sulfur isotope 'mantle array' in chemical geodynamics. *Earth and Planetary Science Letters* **417**: 28-39.
- Lee C.-T. A., Luffi P., Le Roux V., Dasgupta R., Albarede F., Leeman W. P. (2010) The redox state of arc mantle using Zn/Fe systematics. *Nature* **468**: 681-685.
- Lee C.-T. A., Leeman W. P., Canil D., and Li Z.-X. A. (2005) Similar V/Sc Systematics in MORB and Arc Basalts: Implications for the Oxygen Fugacities of their Mantle Source Regions. *Journal of Petrology* **46**(11): 2313-2336.
- Le Voyer M., Cottrell E., Kelley K. A., Brounce M. and Hauri E. H. (2015) The effect of primary versus secondary processes on the volatile content of MORB glasses: An example from the equatorial Mid-Atlantic Ridge (5°N-3°S). *J. Geophys. Res.* **120**, 125–144.
- Lindsley D. H. (Ed.). 1991. Oxygen Barometry of Spinel Peridotites. In B.R. Frost (Author), *Reviews in Mineralogy and Geochemistry* (Vol. 25, 417-432). Mineralogical Society of America.
- Madureira, P., Moreira, M., Mata, J., Nunes, J.C., Gautheron, C., Lourenço, N., Carvalho, R., de Abreu, M.P. (2014). Helium isotope systematics in the vicinity of the Azores triple junction: Constraints on the Azores geodynamics. *Chemical Geology* **372**: 62-71.
- Matzen A. K., Wood B. J., Baker M. B., Stolper E. M. (2017). The roles of pyroxenite and peridotite in the mantle sources of oceanic basalts. *Nature Geoscience* **10**: 530-535.
- McDonough W. F., Sun S.-S. (1995) The composition of the Earth. *Chemical Geology* **120**: 223-253.
- Moreira M., Kanzari A., Madureira P. (2012). Helium and neon isotopes in São Miguel island basalts, Azores Archipelago: new constraints on the "low  $^3\text{He}$ " hotspot origin. *Chemical Geology* **322**: 91-98.
- Moreira, M., Doucelance, R., Dupré, B., Kurz, M., Allègre, C.J. (1999). Helium and lead isotope geochemistry in the Azores archipelago. *Earth and Planetary Science Letters* **169**, 189–205.
- Moussallam Y. *et al.* (2019) Mantle Plumes are oxidized. *Earth and Planetary Science Letters* **527**, 115798.
- Moussallam Y., Edmonds M., Scaillet B., Peters N., Gennaro E., Sides I. and Oppenheimer C. (2016) The impact of degassing on the oxidation state of basaltic magmas: A case study of Kīlauea volcano. *Earth Planet. Sci. Lett.* **450**, 317–325.
- Moussallam Y., Oppenheimer C., Scaillet B., Gaillard F., Kyle P., Peters N., Hartley M., Berlo K. and Donovan A. (2014) Tracking the changing oxidation state of Erebus magmas, from

- mantle to surface, driven by magma ascent and degassing. *Earth Planet. Sci. Lett.* **393**, 200–209.
- Mundl A., Touboul M., Jackson M. G., Day J. M. D., Kurz M. D., Lekic V., Helz R. T., Walker R. J. (2017). Tungsten-182 heterogeneity in modern ocean island basalts. *Science* **356**: 66-69.
- Mundl-Petermeier A., Walker, R. J., Fischer, R. A., Lekic, V., Jackson, M. G., Kurz, M. D. (2020). Anomalous  $^{182}\text{W}$  in high  $^3\text{He}/^4\text{He}$  ocean island basalts: Fingerprints of Earth's core? *Geochimica et Cosmochimica Acta* **271**: 194-211.
- Mungall J. E., Hanley J. J., Arndt N. T., Debecdelievre A. (2006). Evidence from meimechites and other low-degree mantle melts for redox controls on mantle-crust fractionation of platinum-group elements. *PNAS* **103**(34): 12695-12700.
- Nicklas R. W., Day J. M. D., Vaci Z., Udry A., Liu Y., Tait K. T. (2021). Uniform Ambient Mantle Oxygen Fugacity and a Highly Oxidized Lithospheric Mantle on Mars. *Earth and Planetary Science Letters* **564**: 116876.
- Nicklas R. W., Puchtel I. S., Ash R. D., Piccoli P. M., Hanski E., Nisbet E. G., Waterton P, M., Pearson D. G., Anbar A. D. (2019) Secular Mantle Oxidation across the Archean-Proterozoic Boundary: Evidence from V Partitioning in Komatiites and Picrites. *Geochimica et Cosmochimica Acta* **250**: 49-75.
- Nicklas R. W., Puchtel I. S., Ash R. D. (2018). Redox state of the Archean mantle: Evidence from V partitioning in 3.5–2.4 Ga komatiites. *Geochim. Cosmochim. Acta* **222**, 447–466.
- Novella D., MacLennan J., Shorttle O., Prytulak J., Murton B. J. (2020). A multi-proxy investigation of mantle oxygen fugacity along the Reykjanes Ridge. *Earth and Planetary Science Letters* **531**: 115973.
- Padron-Navarta J. A., Sanchez-Vizcaino V. L., Garrido C. J., Gomez-Pugnaire M. T. (2011) Metamorphic record of high-pressure dehydration of antigorite serpentinite to chlorite harzburgite in a subduction setting (Cerro del Almirez, Nevado-Filabride Complex, Southern Spain). *J. Petrol.* **52**, 2047–2078.
- Parai R., Mukhopadhyay S., Lassiter J. C. (2009). New constraints on the HIMU mantle from neon and helium compositions of basalts from the Cook-Austral Islands. *Earth and Planetary Science Letters* **277**: 253-261.
- Pringle E. A., Moynier F., Savage P. S., Jackson M. G., Moreira M., Day J. M. D. (2016). Silicon isotopes reveal recycled altered oceanic crust in the mantle sources of Ocean Island Basalts. *Geochimica et Cosmochimica Acta* **189**: 282-295.
- Rudnick R. L., Gao S. (2003). The composition of the continental crust, in *The Crust*, vol. 3, edited by R. L. Rudnick, p. 1-64, Elsevier Sci., New York.

- Ryabchikov I. D., Ntaflos T., Kurat G., Kogarko L. N. (1995). Glass-bearing xenoliths from Cape Verde: evidence for a hot rising mantle jet. *Mineralogy and Petrology* **55**: 217-237.
- Salters V. J. M., Stracke A. (2004). Composition of the depleted mantle. *Geochemistry, Geophysics, Geosystems* **5**(5).
- Shorttle O., Moussallam Y., Hartley M. E., Maclennan J., Edmonds M., Murton B. J. (2015). Fe-XANES analyses of Reykjanes Ridge basalts: Implications for oceanic crust's role in the solid Earth oxygen cycle. *Earth and Planetary Science Letters* **427**: 272-285.
- Sobolev A. V., Hofmann A. W., Kuzmin D. V., Yaxley G. M., Arndt N. T., Chung S.-L., Danyushevsky L. V., Elliott T., Frey F. A., Garcia M. O., Gurenko A. A., Kamenetsky V. S., Kerr A. C., Krivolutskaya N. A., Matvienkov V. V., Nikogosian I. K., Rocholl A., Sigurdsson I. A., Sushchevskaya N. M., Teklay M. (2007). The Amount of Recycled Crust in Sources of Mantle-Derived Melts. *Science* **316**: 412-417.
- Sobolev A. V., Hofmann A. W., Sobolev S. V., Nikogosian I. K. (2005) An olivine-free mantle source of Hawaiian shield basalts. *Nature* **434**: 590-597.
- Stracke A., Genske F., Berndt J., Koorneef J. (2019) Ubiquitous ultra-depleted domains in Earth's mantle. *Nature Geoscience* **12**: 851-855.
- Stracke A., Hofmann, A. W., Hart, S. R. (2005) FOZO, HIMU, and the rest of the mantle zoo. *Geochemistry, Geophysics, Geosystems* **6**(5).
- Tang M., Erdman M., Eldridge G., Lee C.-T. A. (2018) The redox "filter" beneath magmatic orogens and the formation of continental crust. *Scientific Advances* **4**(5): 1-7.
- Taracsak Z., Hartley M. E., Burgess R., Edmonds M., Iddon F., Longpre M.-A. (2019). High fluxes of deep volatiles from ocean island volcanoes: Insights from El Hierro, Canary Islands. *Geochimica et Cosmochimica Acta* **258**: 19-36.
- Wang J., Xiong X., Takahashi E., Zhang L., Li L., Liu X. (2019). Oxidation State of Arc Mantle Revealed by Partitioning of V, Sc and Ti Between Mantle Minerals and Basaltic Melts. *Journal of Geophysical Research: Solid Earth* **124**: 4617-4638.
- Waters C. L., Day, J. M. D., Watanabe, S., Sayit, K., Zanon, V., Olson, K. M., Hanan, B. B., Widom, E. (2020). Sulfide mantle source heterogeneity recorded in basaltic lavas from the Azores. *Geochimica et Cosmochimica Acta* **268**: 422-445.
- Waters L. E. and Lange R. A. (2016) No effect of H<sub>2</sub>O degassing on the oxidation state of magmatic liquids. *Earth Planet. Sci. Lett.* **447**, 48–59.
- Wood B. J., Walter M. J., Wade J. (2006). Accretion of the Earth and segregation of its core. *Nature*, **441**(7095): 825-833.

- Workman R. K., Hart S. R. (2005). Major and trace element composition of the depleted MORB mantle (DMM). *Earth and Planetary Science Letters* **231**: 53-72.
- Workman R. K., Hart S. R., Jackson M., Regelous M., Farley K. A., Blusztajn J., Kurz M., Staudigel H. (2004). Recycled metasomatized lithosphere as the origin of the Enriched Mantle II (EM2) endmember: evidence from the Samoan volcanic chain. *Geochem. Geophys. Geosys.* **5**(4): 1-44.
- Williams H. M., Bizimis M. (2014). Iron isotope tracing of mantle heterogeneity within the source regions of oceanic basalts. *Earth and Planetary Science Letters* **404**: 396-407.
- Woodhead J. D. (1996) Extreme HIMU in an oceanic setting: the geochemistry of Mangaia Island (Polynesia), and temporal evolution of the Cook-Austral hotspot. *Journal of Volcanology and Geothermal Research* **72**: 1-19.
- Zhang H. L., Cottrell E., Solheid P. A., Kelley K. A., Hirschmann M. M. (2018) Determination of Fe<sup>3+</sup>/ΣFe of XANES basaltic glass standards by Mössbauer spectroscopy and its application to the oxidation state of iron in MORB. *Chemical Geology* **479**: 166-175.
- Zindler A., Hart S. (1986) Chemical Geodynamics. *Ann. Rev. Earth Planet. Sci.* **14**: 493-571.

Figure 1

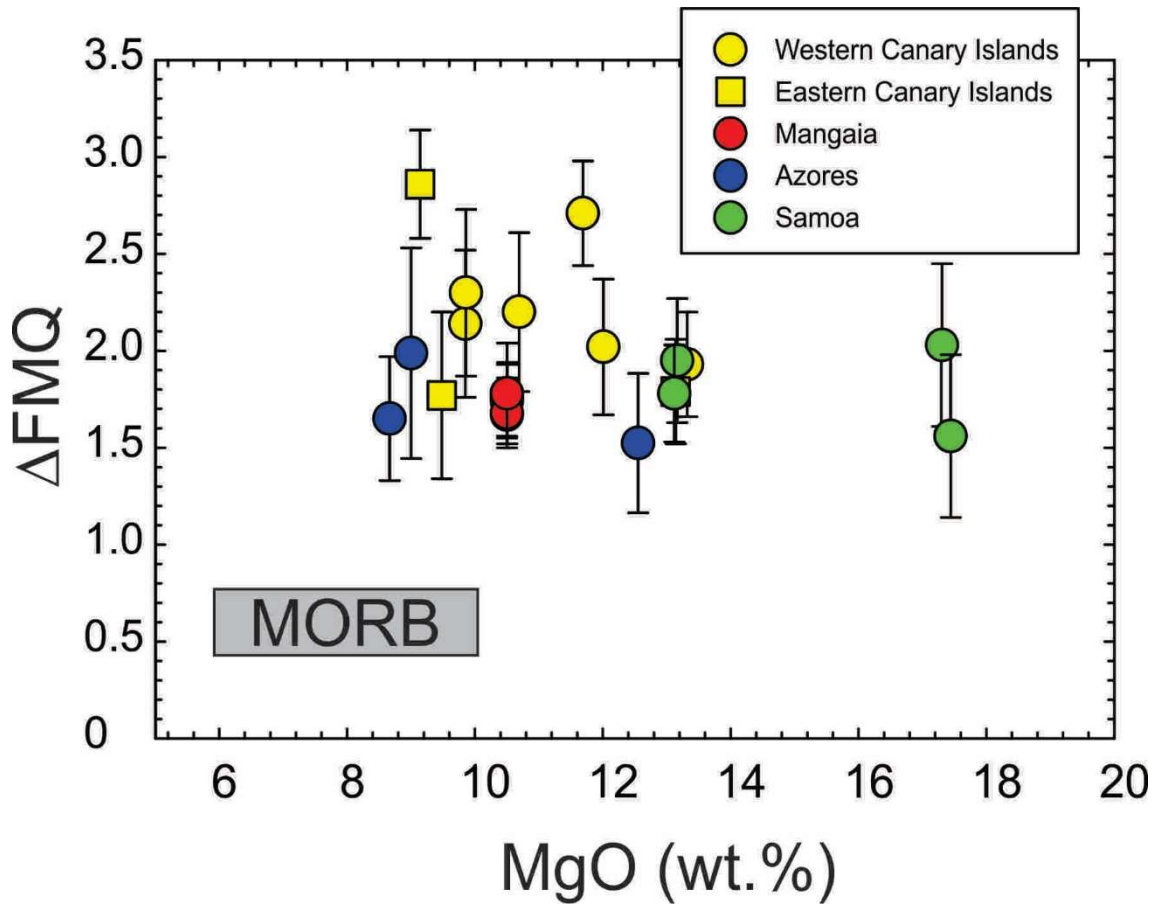


Figure 2

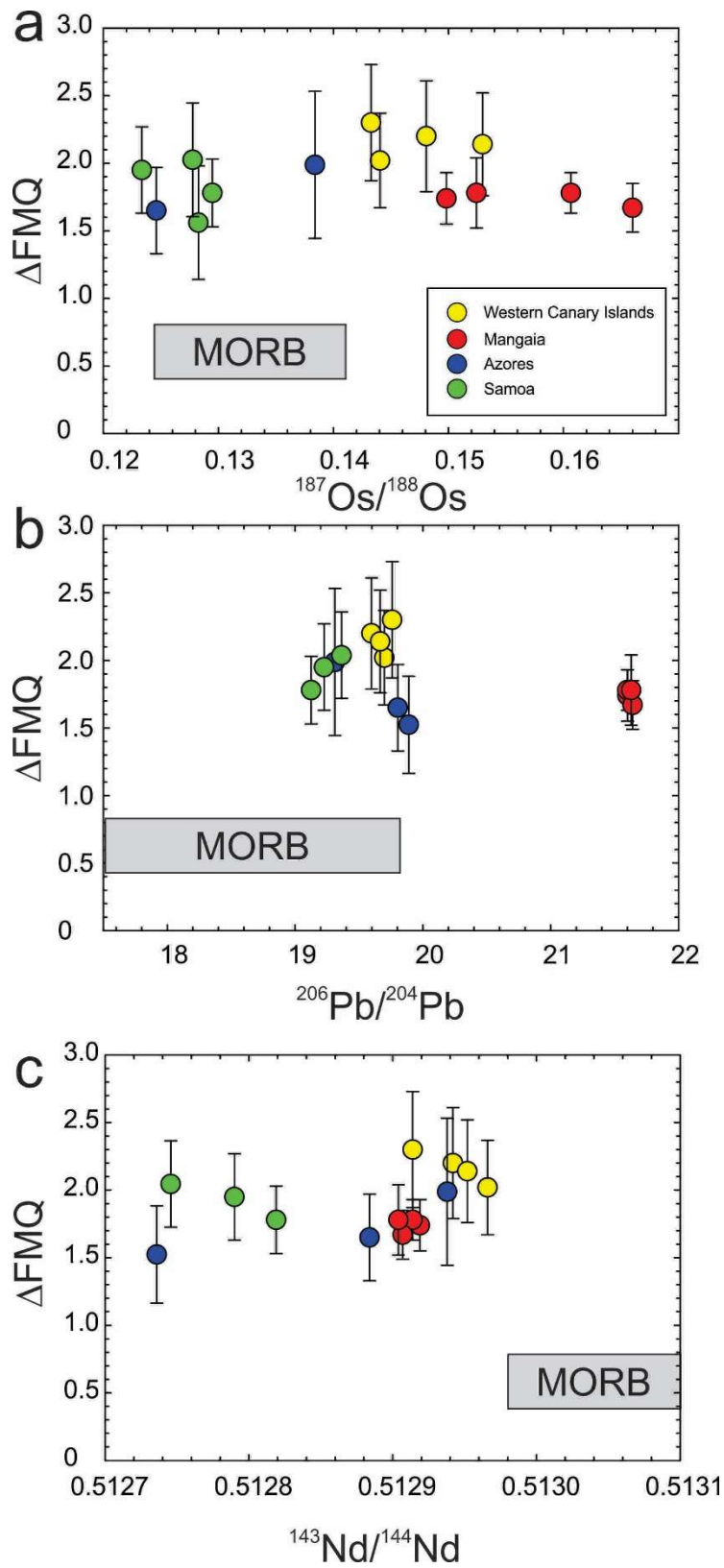


Figure 3.

